Climate Change Economics and Heat Transport across the Globe: Spatial-DSICE

Yongyang Cai, The Ohio State University

William Brock, University of Wisconsin and University of Missouri

Anastasios Xepapadeas, Athens University

Climate Change Economics and Heat Transport across the Globe: Spatial-DSICE [*]

Yongyang Cai[†]   William Brock[‡]   Anastasios Xepapadeas[§]

December 6, 2016

Abstract

This paper extends the stochastic DSICE model of Cai et al. (Cai et al. 2015a, 2015b) to include the case of spatial transport of heat and moisture from the Equator to the Poles. This well-known and important phenomenon in climate science has been neglected in popular IAM's, e.g. RICE and DICE (Nordhaus 2010, 2013). Spatial transport leads to another well-known phenomenon in climate science called polar amplification where a one degree increase in the global yearly mean temperature anomaly causes a more than one degree increase of the yearly mean temperature anomaly in the high latitudes (Langen and Alexeev 2007). This extension allows us to compare the optimal paths of key quantities like the Social Cost of Carbon (SCC), emissions, abatement, and damages and their uncertainty bands when

[†]The Ohio State University. cai.619@osu.edu

[‡]University of Wisconsin and University of Missouri. wbrock@ssc.wisc.edu

[§]Athens University of Economics and Business. xepapad@aueb.gr

1

heat and moisture transport are neglected as in the received literature on IAMs to when this important phenomenon documented by climate science is included. We view our paper as a first step towards adding additional aspects of climate dynamics like heat and moisture transport across latitudes and polar amplification to the existing literature on IAMs.

1   Introduction

A major characteristic of leading Integrated Assessment Models (IAMs) such as RICE-2011 or DICE-2013R (Nordhaus 2010, 2013) is that the geophysical sector of the model determines the mean surface temperature through the carbon cycle, which in turn determines the damage function. Thus damages are related to the mean surface temperature of the planet.

A well-established fact in the science of climate change, however, is that when the climate cools or warms, high latitude regions tend to exaggerate the changes seen at lower latitudes (e.g. Langen and Alexeev 2007; IPCC 2013, p.396). This effect is called polar amplification and indicates that under global warming the temperature at the latitudes closer to the Poles will increase faster than at latitudes nearer to Equator. Polar amplification is especially strong in the Arctic and is sometimes called "Arctic amplification". For example, Bekryaev et al. (2010) document a high-latitude (greater than 60 °N) warming rate of 1.36 degrees centigrade per century from 1875 to 2008. This is a trend almost twice that of the Northern Hemisphere trend of 0.79 degrees centigrade per century.

Polar amplification has been associated with the surface albedo feedback (SAF),[1] but recent research suggests that significant polar amplification may also emerge as a result of atmospheric heat and moisture transport polarwise, even without SAF (Langen and Alexeev 2007). Spatial heat and moisture transport, and the resulting polar amplification, suggest that a better representation of the climate science underlying the IAMs would be a geophysical sector structure which accounts for these phenomena. This implies that, in the IAM output, the surface temperature anomaly will be differentiated across spatial zones of the globe. The spatial temperature differentiation will be important for the economics of climate change because it will provide the impact of polar amplification on the structure of the economic damages. Polar amplification will accelerate the loss of Arctic sea ice, which in turn has consequences for melting land ice. Melting land ice is associated with a potential meltdown of Greenland and West Antarctica ice sheets which might

---

[1]The SAF mechanism can be traced back to Arrhenius (1896).

cause serious global sea level rise. Another source of damage related to polar amplification relates to the thawing of the permafrost, which is expected to bring widespread changes in ecosystems and to damage infrastructure, along with release of greenhouse gases which exist in permafrost carbon stocks (see for example IPCC 2013; Schaefer et al. 2014; Schuur et al. 2015).

Furthermore, recent studies suggest that Arctic amplification is expected to increase the frequency of extreme weather events (Francis and Vavrus 2014; Francis and Skific 2015). Lenton and Schellnhumber's (2007, Figure 1) well-known "burning embers" diagram shows the ranking of tipping elements by order of proximity to the present. Note that the "nearest" three potential tipping points are located in the high latitudes of the Northern Hemisphere (Arctic summer sea ice loss, Greenland ice sheet melt, boreal forest loss). Because of polar amplification in the Arctic each degree increase in planetary yearly mean temperature leads to approximately two degrees increase in the Arctic latitudes. Indeed Livinia and Lenton (2013) say, "Examination of satellite data for Arctic sea-ice area reveals an abrupt increase in the amplitude of seasonal variability in 2007 that has persisted since then." Hence this is a type of tipping event that has already occurred and may have been caused earlier because of polar amplification.

Thus natural phenomena occurring in high latitudes, due to spatial heat and moisture transport, can cause economic damages in lower latitudes. These spatial impacts, which could have important implications for climate change policies, are not embodied in the current generation of IAMs. The RICE model (Nordhaus 2010), the regional version of DICE (Nordhaus 2013), still treats the climate system with the globally average measure of temperature and neglects heat and moisture transport and, especially, polar amplification. The novel contribution of the present paper is to develop an IAM which incorporates spatial impacts associated with heat and moisture transport, along with treatment of uncertainty and tipping points. As far as we know no other IAM treats these issues as we do here. For example, the Dynamic Stochastic Integration of Climate and Economy (DSICE) model of Cai et al. (2015a) is especially well equipped to produce distributions of the Social Cost of Carbon (SCC) so that the impacts of realistic uncertainties

4

on the SCC may be properly assessed, since policy analysis must take into account higher moments of the uncertainty distribution of SCC, not just the mean. To put it another way the SCC must be treated as a stochastic process in order to properly assess the uncertainty in the SCC which is required for risk and uncertainty management. Hence the DSICE model seemed to us to be the natural place to add aspects of climate dynamics like heat and moisture transport across regions and to investigate what difference this extra component of realism makes to the optimal paths of the SCC, optimal emissions in each region, optimal adaptation in each region and optimal tradeoff between economic growth and climate damages in each region. We hasten to note before we begin that our Spatial-DSICE is an optimal planning model and it is beyond the scope of this paper to deal with the free rider problem attacked in Nordhaus's recent paper (Nordhaus 2015). However, we believe that our Spatial-DSICE model will help provide additional technical support for Nordhaus's calculations of the net benefits as well as uncertainty bands surrounding net benefits for countries located in Southern and Northern latitude belts of joining his climate club. Indeed, that task is on our research agenda. At the risk of repeating we go into some more detail below.

The DSICE framework (Cai et al. 2015a, 2015b), is a stochastic generalization of DICE that has been used to compute estimates of uncertainty bands around central values of the SCC, as well as to compute adjustments to the SCC when realistic economic uncertainties are taken seriously and wide differences of projections of potential tipping points from expert opinions may occur. However, DSICE does not consider impact from either regional economics or regional temperatures. Thus in the present paper is to introduce spatial heat and moisture transport which cause polar amplification into the DICE-2013R (Nordhaus and Sztorc 2013) and its stochastic generalization, DSICE. Spatial heat and moisture transport induces a spatial structure into the geophysical sector of DICE and DSICE. We call the resulting IAM a Spatial-DSICE. The Spatial-DSICE is the first, to our knowledge, to introduce the well-known climate dynamics phenomenon of spatial heat/moisture transport into DICE type IAMs where the quantitative impact of including spatial heat/moisture transport can be assessed

5

under realistic uncertainties.[2] By comparing the predictions of the standard DICE with the predictions of the Spatial-DSICE, using the same economic parameters, our purpose is to explore the impacts on the design of climate policy of ignoring the existing spatial transport phenomena. For example, by ignoring spatial transport, do we overestimate or underestimate optimal emission paths, carbon taxes, and the SCC, and what is the impact on the general shape of the uncertainty bands around these paths when heat and moisture transport is neglected? On a more general level, we are trying to bring the geophysical sector of the IAMs closer to current climate science, which will undoubtedly improve the reliability of economic predictions.

Perhaps, more importantly, treating the increase in the temperature anomaly as the same over the whole planet by neglecting polar amplification when the temperature anomaly increases almost twice as much in the high latitudes will understate the projected arrival time of potential tipping points and potential abrupt changes in the Arctic latitudes. Since the higher latitudes in the Northern Hemisphere are where the three "nearest" tipping elements are located (Lenton and Schellnhuber 2007, Figure 1) not taking heat and moisture transport into account will bias estimates of the stochastic "arrival" time of these three potential tipping points, i.e. the hazard function will be biased towards predicting a later arrival of a tipping point time for tipping elements in the high latitudes which are triggered by temperature rise.

In developing the Spatial-DSICE, we follow the two-region approach of Langen and Alexeev (2007) and define two regions: region 1 is the region north of latitude 30°N to 90°N, while region 2 is the region from latitude 90°S (the south pole) to 30°N. Heat and moisture transport takes place northbound from the tropic belt of region 2 towards the 30°N to 90°N belt of region 1, and is ignored for the southern hemisphere for dimension reduction as the polar amplification in the south pole is not as serious as in the north

---

[2]Brock and Xepapadeas (2015) considered a simple deterministic model and showed that by ignoring spatial heat and moisture transport and the resulting polar amplification, the regulator may overestimate or underestimate the tax on GHG emissions. The structure of their economic model is, however, simplified and this makes it difficult to discuss realistic policy options.

pole.

The interaction of the geophysical sector of the Spatial-DSICE with the economic sector is reflected in the damage function. We introduce separate damage functions in each region and allow for damages in region 2 to be caused by an increase in temperature (i.e. polar amplification) in region 1. For example, the increased amplification of the temperature anomaly in the high north latitudes increases the hazard rate of tipping events in the high north latitudes towards earlier arrival times. Hence any associated damages caused to lower latitudes from warming in the higher north latitudes, e.g. increased melting of land ice leading to sea level rise damages in the lower latitudes, will be increased by polar amplification even though the high north latitudes may benefit from additional warming.

The rest of the economic module is based on a two-region differentiation of DICE-2013R (Nordhaus and Sztorc 2013). We model the economic interactions between the two regions with an adjustment cost function; and we allow for adaptation expenses in each region.

We expect that our results will provide new insights regarding the importance of spatial phenomena in climate change policy, and will indicate the potential benefits of bringing IAMs closer to the science of climate change.

The paper is organized as follows. Section 2 builds a deterministic version of Spatial-DSICE, where we calibrate our spatial climate system and economic system based on DICE and RICE as well as data in the other literature like IPCC (2013). Section 3 analyzes results of the deterministic model. Section 4 extends the deterministic model to be stochastic, i.e., Spatial-DSICE, using a tipping point as one representative risk and Epstein–Zin preferences to address the smoothness of consumption across time and risk aversion following DSICE. Section 5 discusses the results of Spatial-DSICE. Section 6 concludes.

2   Deterministic Model

Our deterministic model is based on DICE-2013R (Nordhaus 2013; Nordhaus and Sztorc 2013), which maximizes social welfare with tradeoffs between

Figure 1: The Spatial-DSICE model
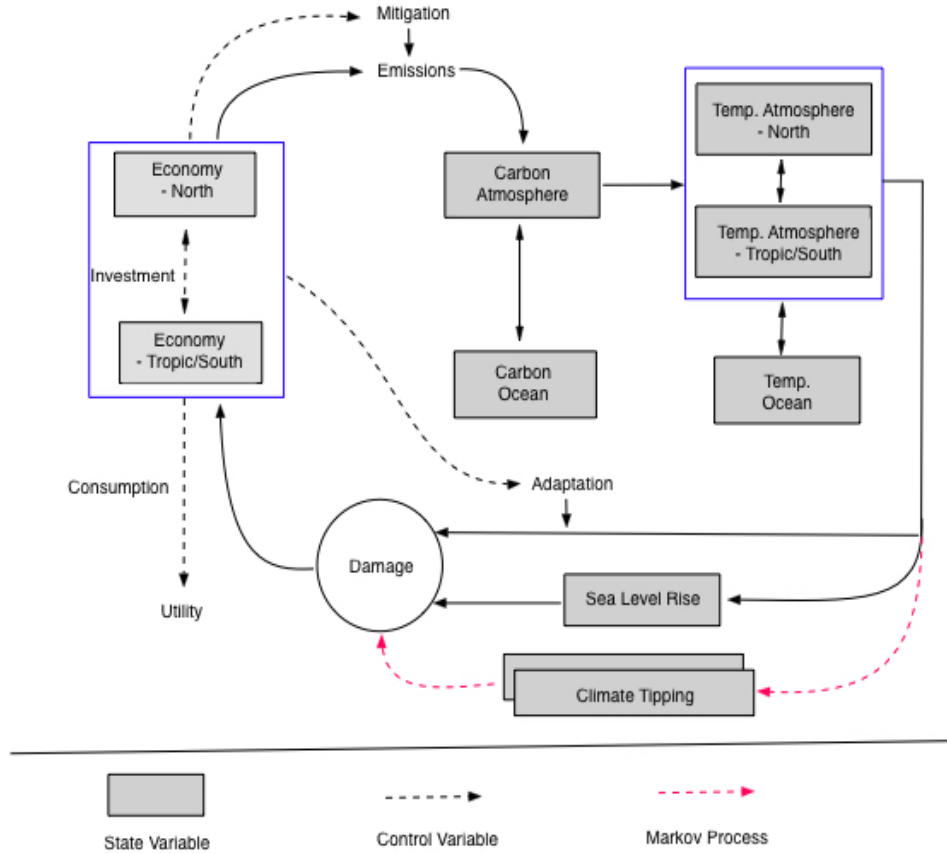
carbon dioxide (CO_2) abatement, consumption, and investment. Our model has been augmented relative to DICE-2013R to include adaptation to climate change following de Bruin et al (2009). The Spatial-DSICE model has two regions: the first one (indexed with $i = 1$) is the north region from latitude 30°N to 90°N, the second one is the left tropic/south region from latitude 90°S to 30°N. We model it as a social planner problem with both economic and climate interaction between two regions. The big picture of the model setup is depicted in Figure 1 (ignoring the stochastic climate tipping part in the figure), and we describe its details below.

2.1 The Climate System

The climate system contains three modules: carbon cycle, temperature system, and sea level rise (SLR).

2.1.1 Carbon cycle

DICE-2013R uses three-layer carbon concentrations: atmospheric carbon, carbon in the upper ocean, and carbon in the deep ocean. However, from our calibration, we find that the mass of carbon concentration in the dean ocean is almost invariant because the interaction coefficient between the upper ocean and the deep ocean is nearly zero. This reflects the saturation of ocean absorption with higher temperatures and carbon content. This tells us that we can drop the deep ocean in our model. Thus, we use $\mathbf{M}_t = (M_t^{\mathrm{AT}}, M_t^{\mathrm{UO}})^\top$ to represent the carbon concentration in the atmosphere and the upper ocean, and then the two-layer carbon cycle system is

$$\mathbf{M}_{t+1} = \boldsymbol{\Phi}_{\mathrm{M}} \mathbf{M}_t + (E_t, 0)^\top, \tag{1}$$

where E_t is the global carbon emission (billions of metric tons) and

$$\boldsymbol{\Phi}_{\mathrm{M}} = \begin{bmatrix} 1 - \phi_{12} & \phi_{21} \\ \phi_{12} & 1 - \phi_{21} \end{bmatrix} \tag{2}$$

The parameters ϕ_{12} and ϕ_{21} are calibrated against four RCP scenarios: using each RCP emission scenario as the input E_t, our carbon cycle outputs a path of atmospheric carbon concentration, and MAGICC also provides a corresponding atmospheric carbon concentration path. At the same time, we also calibrate ϕ_{12} and ϕ_{21} so that our atmospheric carbon concentration path generated with the optimal DICE emission path matches the corresponding optimal DICE atmospheric carbon concentration path (see Figure 2).

9

Figure 2: Fitting Atmospheric Carbon Concentration
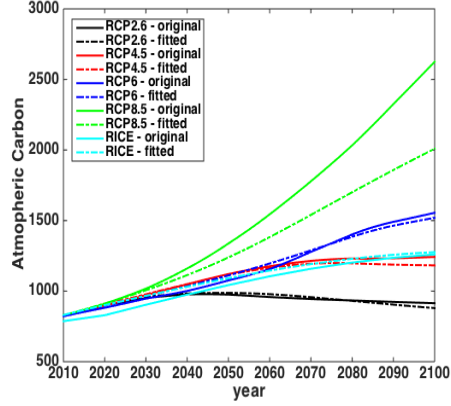
2.1.2 Temperature subsystem

The global radiative forcing representing the CO_2 concentrations impact on the surface temperature of the globe (watts per square meter from 1900) is

$$F_t = \eta \log_2 \left(M_t^{\text{AT}} / M_*^{\text{AT}} \right) + F_t^{\text{EX}}, \tag{3}$$

with $\eta = 3.8$ as in DICE-2013R, where F_t^{EX} is the global exogenous radiative forcing.

We use $\mathbf{T}_t = (T_{t,1}^{\text{AT}}, T_{t,2}^{\text{AT}}, T_t^{\text{OC}})^\top$ to represent the temperature anomaly (relative to 1900 levels) in the atmosphere (two regions) and the global ocean. Thus, the temperature system is

$$\mathbf{T}_{t+1} = \mathbf{\Phi}_{\text{T}} \mathbf{T}_t + \xi_1 F_t (1, 1, 0)^\top, \tag{4}$$

where we assume that the global radiative forcing has the same effect on both regions, and

$$\mathbf{\Phi}_{\text{T}} = \begin{bmatrix} 1 - B - \gamma_1 - \xi_2 & \gamma_1 + \gamma_2 & \xi_2 \\ \gamma_1 & 1 - B - \gamma_1 - \gamma_2 - \xi_2 & \xi_2 \\ \xi_3 & \xi_3 & 1 - 2\xi_3 \end{bmatrix}$$

10

Figure 3: Fitting Surface Temperature of RCP or RICE scenarios
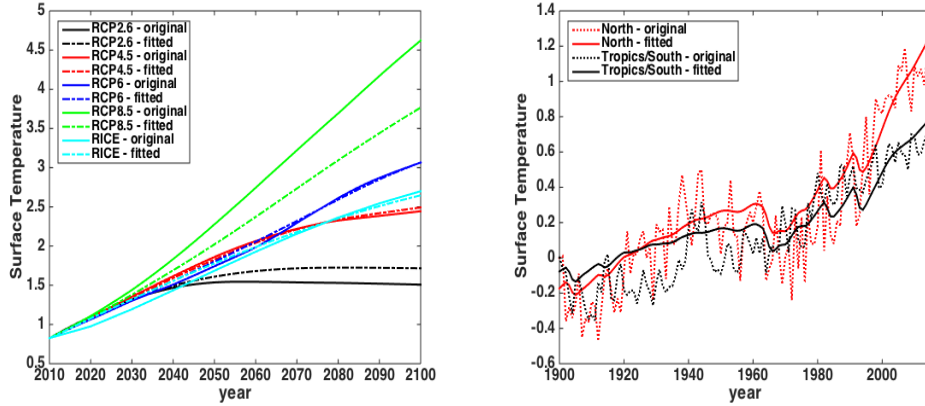
We calibrate $B, \xi_1, \xi_2, \xi_3, \gamma_1, \gamma_2$ by

- matching four RCP globally average atmospheric temperature pathways: using each RCP emission pathway as the input, our carbon cycle, radiative forcing and temperature system provide paths of atmospheric temperatures in two regions, we average two paths to get a globally average atmospheric temperature path, whilst MAGICC also provides a corresponding globally average atmospheric temperature path. See the left panel of Figure 3).

- matching the RICE optimal climate pathway. See the left panel of Figure 3).

- matching the historical spatial temperatures in 1900-2015 from GISS (see the right panel of Figure 3)

- matching the spatial temperatures in 2081-2100 to the ones given in IPCC (2013). See Figure 4.

2.1.3 Sea Level Rise

Sea level rise (SLR) is a serious problem caused by global warming. From IPCC (2013) Table 4.1, if the whole Antarctic ice sheet melts, it will lead to

Figure 4: Spatial temperature using RCP or RICE radiative forcing scenarios
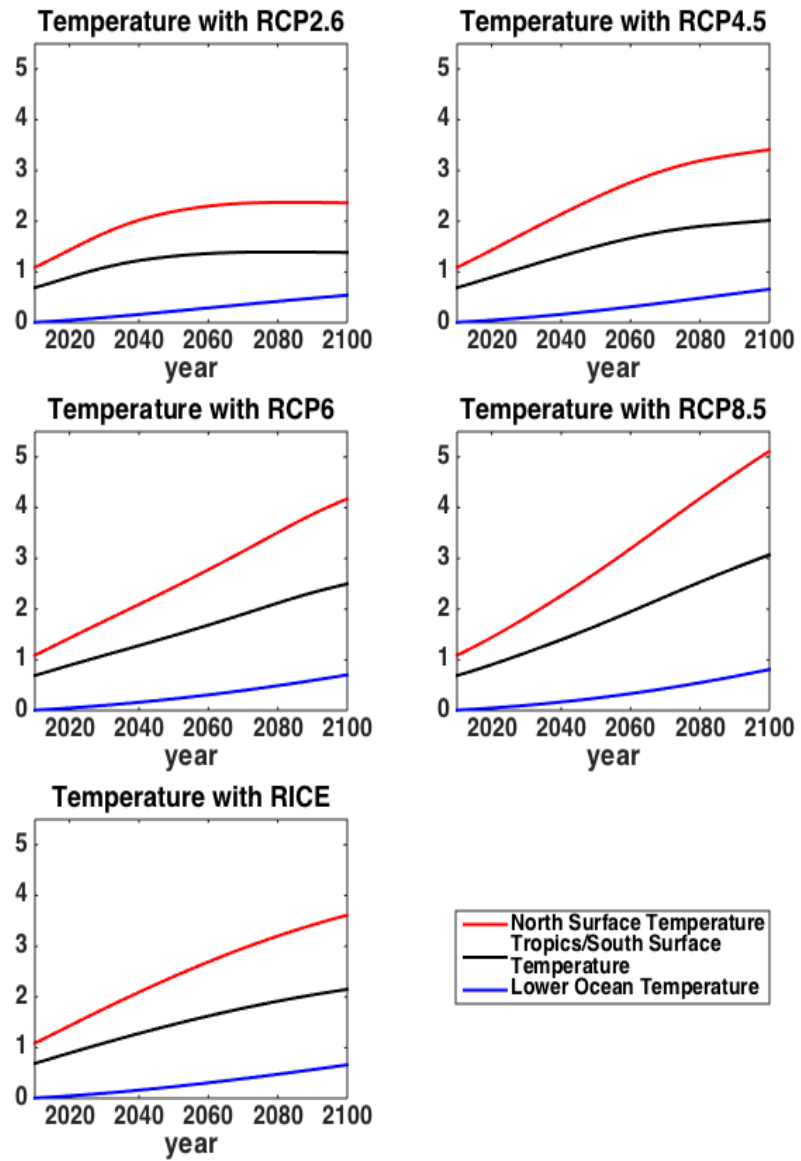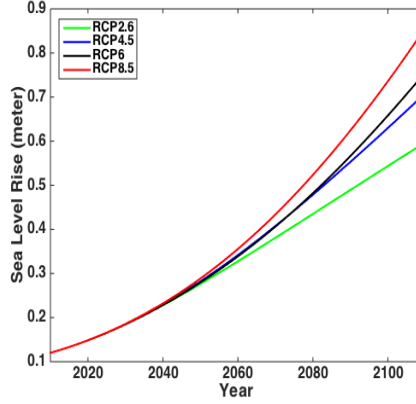
Figure 5: Fitting SLR

about 58 meters sea level rise; and if the whole Greenland ice sheet melts, it will have more than 7 meters sea level rise. Moreover, once ice sheet collapses, it is irreversible for millennia even if forcing is reversed (IPCC 2013, Table 12.4). Nerem et al (2010) estimate the global mean sea level rise is around 3.2 mm per year (mm/yr) in the last two decades. IPCC (2013) Table 13.5 shows that SLR in 2100 are from around 0.44 meters for RCP2.6 to around 0.74 meters for RCP8.5, while the likely range of SLR in 2100 is from 0.3 meters to 1 meter. Except measuring in yearly rates, IPCC (2013) Figure 13.14 shows that the likely range of SLR is from 1 to 3 meters per Celsius of globally average surface temperature increase if the warming is sustained for millennia.

We let the sea level rise S_t to be endogenous and irreversible. We assume that its transition law depends on contemporaneous north surface temperature so that a higher temperature implies a higher rate of SLR. Thus, we let

$$S_{t+1} = S_t + \pi_5 T_{t,1}^{\mathrm{TA}} \tag{5}$$

where π_5 is calibrated using the SLR data for four RCP scenarios in Table 13.5 and Figure 13.11 of IPCC (2013). Figure 5 shows our fitted SLR paths which are close to the median projections in Figure 13.11(a) of IPCC (2013).

13

2.2 The Economic System

2.2.1 Production

We use the annual analogs of the exogenous paths of DICE-2013R in five-year time units, including the carbon intensity technology factor σ_t, and the adjusted cost for backstop $\theta_{1,t}$. We use region-specific total productivity factor (TFP) $A_{t,i}$. Sachs (2010) stresses on ecological specific technical progress and lists five reasons why TFP's in low latitude zones tend to be smaller than temperate latitude zones. Of course there are exceptions as Sachs points out (e.g. Hong Kong and Singapore, and, now, lower latitude parts of China and parallel parts of "Asian Tigers"). However, theory suggests that the economies that are "behind" should grow faster than the leaders because the leaders have already done the "heavy lifting" of the TFP R&D which presumably the followers could copy. For example, Sachs and McArthur (2002) discuss the transition from "adopter" to "innovator" for countries. Desmet and Rossi-Hansberg (2014, 2015) also discuss the spatial diffusion of technology with no migration or free migration.

Let $T_{t,i}^{\mathrm{AT}}$ be temperature in the atmosphere at time t and region i. The gross output at time t is

$$\mathcal{Y}_{t,i} \equiv A_{t,i} K_{t,i}^{\alpha} L_{t,i}^{1-\alpha}, \tag{6}$$

with $\alpha = 0.3$ and $L_{t,i}$ is exogenous population at time t and region i aggregated from RICE.[3] We let

$$A_{t,i} = A_{0,i} \exp\left(\alpha_i^A \left(1 - \exp\left(-d_i^A t\right)\right) / d_i^A\right)$$

where $A_{0,i}$, α_i^A and d_i^A are calibrated to match the productivity path in region i which are computed from RICE by aggregating across the RICE subregions in region i[4] (see Figure 6).

---

[3]For region i and time t, we sum up population over the RICE subregions locating in region i (if one RICE subregion locates across our border lines 30°N or 30°S, then we give a rough estimate with the ratio of land of the subregion locating in the region i).

[4]We first estimate $K_{t,i}$, $L_{t,i}$ and $\mathcal{Y}_{t,i}$ by summing over those in RICE subregions locating in our region i for each time t, and then compute the total factor productivity paths

Figure 6: Fitting Total Factor Productivity
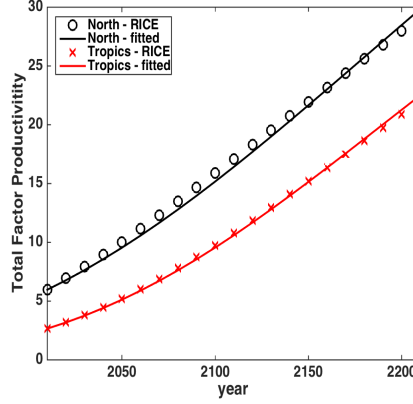
2.2.2 Damages

We follow RICE to let

$$D_{t,i}^{\mathrm{S}} = \pi_{1,i} S_t + \pi_{2,i} S_t^2$$

reflect the damage in fraction of output from sea level rise (SLR) S_t. We calibrate $\pi_{1,i}$ and $\pi_{2,i}$ to match the damage from surface temperature change above the initial year (i.e., 2010) level which are computed from RICE.[5]See Figure 7.

We follow DICE and RICE to let

$$D_{t,i}^{\mathrm{T}} = \pi_{3,i} T_{t,i}^{\mathrm{AT}} + \pi_{4,i} (T_{t,i}^{\mathrm{AT}})^2 \tag{7}$$

reflect the fraction of non-SLR damage to output from surface temperature change above the 1900 level. We calibrate $\pi_{3,i}$ and $\pi_{4,i}$ to match the damage from surface temperature anomaly which are computed from RICE.[6]See

---

$A_{t,i} = \mathcal{Y}_{t,i}/(K_{t,i}^{\alpha} L_{t,i}^{1-\alpha})$ for region i .

[5]We estimate $\mathcal{Y}_{t,i}$ and $\mathcal{D}_{t,i}^{\mathrm{S}} = D_{t,i}^{\mathrm{S}} \mathcal{Y}_{t,i}$ by summing over those in RICE regions locating in our region i for each time t, and then compute $D_{t,i}^{\mathrm{S}} = \mathcal{D}_{t,i}^{\mathrm{S}}/\mathcal{Y}_{t,i}$ for region i . With the data of the sea level rise path in RICE. and $D_{t,i}^{\mathrm{S}}$, we then calibrate $\pi_{1,i}$ and $\pi_{2,i}$ so that the equation (7) holds.

[6]We use the radiative forcing path in RICE to estimate $T_{t,i}^{\mathrm{AT}}$ using our calibrated climate equation (4). We also estimate $\mathcal{Y}_{t,i}$ and $\mathcal{D}_{t,i}^{\mathrm{T}} = D_{t,i}^{\mathrm{T}} \mathcal{Y}_{t,i}$ by summing over those in RICE regions locating in our region i for each time t, and then compute $D_{t,i}^{\mathrm{T}} = \mathcal{D}_{t,i}^{\mathrm{T}}/\mathcal{Y}_{t,i}$
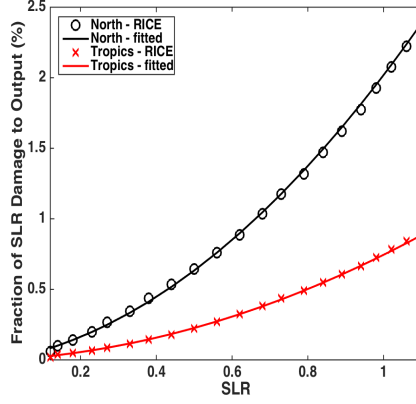
Figure 7: Fitting SLR damage to output

Figure 8.

We include an adaptation choice variable $P_{t,i}$ for each region in our model as in de Bruin et al. (2009). The output net of climate damage is

$$Y_{t,i} \equiv \frac{\mathcal{Y}_{t,i}}{1 + D^{\mathrm{S}}_{t,i} + (1 - P_{t,i})D^{\mathrm{T}}_{t,i}}, \tag{8}$$

where $P_{t,i} \in [0,1]$ is the adaptation rate for the temperature increase, but not for SLR.

2.2.3 Emissions, Mitigation, and Adaptation

The global carbon emission at time t is

$$E_t \equiv \sum_{i=1}^{2} E^{\mathrm{Ind}}_{t,i} + E^{\mathrm{Land}}_t,$$

where E^{Land}_t is the global carbon emission from biological processes, and

$$E^{\mathrm{Ind}}_{t,i} = \sigma_{t,i}(1 - \mu_{t,i})\mathcal{Y}_{t,i}$$

for region i . With the data of $T^{\mathrm{AT}}_{t,i}$ and $D^{\mathrm{T}}_{t,i}$, we then calibrate $\pi_{1,i}$ and $\pi_{2,i}$ so that the equation (7) holds.

16

Figure 8: Fitting non-SLR damage to output
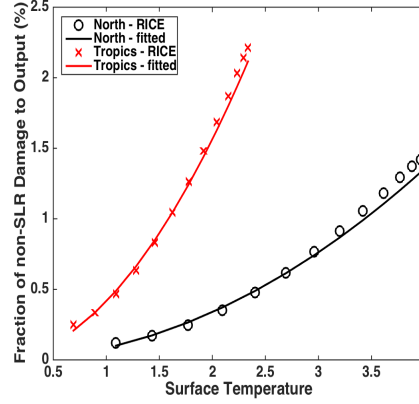
is the industrial emission, where $\mu_{t,i} \in [0,1]$ is an emission control rate and $\sigma_{t,i}$ is the carbon intensity in region i. We let

$$\sigma_{t,i} = \sigma_{0,i} \exp\left(\alpha_i^{\sigma}\left(1 - \exp\left(-d_i^{\sigma} t\right)\right)/d_i^{\sigma}\right)$$

where $\sigma_{0,i}$, α_i^{σ} and d_i^{σ} are calibrated to match the carbon intensity path in region i which are computed from RICE by aggregating across the RICE subregions in region i[7] (see Figure 9).

We follow DICE-2013R to assume that mitigation expenditure is

$$\Psi_{t,i} \equiv \theta_{1,t,i} \mu_{t,i}^{\theta_2} Y_{t,i}$$

where $\theta_{1,t,i}$ is the abatement cost in fractions of output in region i at time t. We use the DICE/RICE form to define

$$\theta_{1,t,i} = b_{0,i} \exp\left(-\alpha_i^b t\right) \sigma_{t,i}/\theta_2$$

where α_i^b and θ_2 are parameters given by RICE, and $b_{0,i}$ is the initial backstop

---

[7]We use the Business-As-Usual (BAU) results (i.e., with $\mu_{t,i} \equiv 0$) of RICE to estimate the carbon intensity paths. We first estimate $E_{t,i}^{\mathrm{Ind}}$ and $\mathcal{Y}_{t,i}$ under BAU by summing over those in RICE subregions locating in our region i for each time t, and then compute the carbon intensity paths $\sigma_{t,i} = E_{t,i}^{\mathrm{Ind}}/\mathcal{Y}_{t,i}$ for region i .

Figure 9: Fitting Carbon Intensity
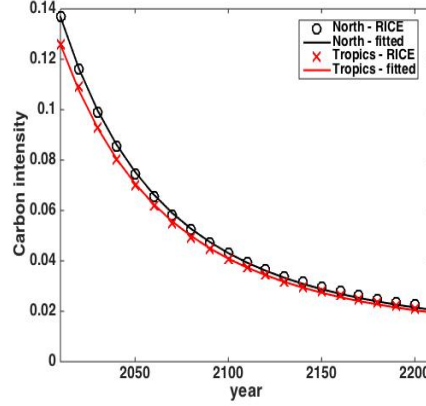
price in region i.

We follow de Bruin et al. (2009) to assume that adaptation expenditure is

$$\Upsilon_{t,i} \equiv \eta_1 P_{t,i}^{\eta_2} Y_{t,i}$$

with $\eta_1 = 0.115$ and $\eta_2 = 3.6$. Let $\widehat{Y}_{t,i}$ denote the output net of climate damage, mitigation expenditure and adaptation cost, that is,

$$\widehat{Y}_{t,i} = Y_{t,i} - \Psi_{t,i} - \Upsilon_{t,i}$$

2.2.4 Economic interaction

In the economic system, each region has a capital state variable $K_{t,i}$, and its law of motion is:

$$K_{t+1,i} = (1 - \delta)K_{t,i} + I_{t,i} \tag{9}$$

where $I_{t,i}$ is investment in region i. Between two regions, there are economic interaction cost such as tariff between countries. For example, Eaton and Kortum (2002) find that if all countries (in their data set) collectively remove tariffs, then most countries will gain around 1% of output with mobile labor, and less than 0.5% with immobile labor. We then model the economic

18

interaction between two regions with the following adjustment cost function:

$$\Gamma_{t,i} \equiv \frac{\zeta}{2} K_{t,i} \left(\frac{I_{t,i} + c_{t,i} L_{t,i}}{\widehat{Y}_{t,i}} - 1 \right)^2 \tag{10}$$

where ζ is the intensity of the friction ($\zeta = 0$ means the open economy, and a large ζ approximates the closed economy with $\widehat{Y}_{t,i} = I_{t,i} + c_{t,i} L_{t,i}$). Anderson and van Wincoop (2001) discuss border barriers and how costly they are. Similar adjustment cost functions have been used in Den Haan et al. (2011) and Goulder et al. (2014). The economic interaction cost also includes the cost for avoiding carbon leakage between two regions.

The market clearing condition is

$$\sum_{i=1}^{2} (I_{t,i} + c_{t,i} L_{t,i} + \Gamma_{t,i}) = \sum_{i=1}^{2} \widehat{Y}_{t,i} \tag{11}$$

2.2.5 Welfare and Model

The total social welfare is

$$\sum_{t=0}^{\infty} \beta^t \sum_{i=1}^{2} \tau_{t,i} u(c_{t,i}) L_{t,i},$$

where β is the discount factor, $c_{t,i}$ are per-capita consumption, $\tau_{t,i}$ are weights for $i = 1, 2$, and u is a per-capita utility function:

$$u(c) = \frac{c^{1-\frac{1}{\psi}}}{1 - \frac{1}{\psi}} \tag{12}$$

where ψ is intertemporal elasticity of substitution (IES) whose inverse is also the elasticity of marginal utility across time.

Therefore, the social planner's problem is

$$\max_{I_{t,i}, c_{t,i}, \mu_{t,i}, P_{t,i}} \quad \sum_{t=0}^{\infty} \beta^t \sum_{i=1}^{2} \tau_{t,i} u(c_{t,i}) L_{t,i} \tag{13}$$

19

subject to the transition laws (1), (4), (5), (9), and the market clearing constraint (11). It has eight state variables: $K_{t,1}$, $K_{t,2}$, S_t, $\mathbf{M}_t$ (two-dimensional vector), and $\mathbf{T}_t$ (three-dimensional vector), as well as eight control variables $(I_{t,1}, I_{t,2}, c_{t,1}, c_{t,2}, \mu_{t,1}, \mu_{t,2}, P_{t,1}, P_{t,2})$ at each time t. We calibrate IES at 0.667 and $\tau_{t,i}$ so that our consumption paths from solving (13) with the closed economy are close to RICE's consumption paths in two regions, as RICE assumes the closed economy.

3 Results for Deterministic Model

Since the choice of discount factor $\beta = 0.985$ makes the welfare after 300 years have little impact on the first 100 years' solutions, we approximate the infinite-horizon problem (13) by a finite-horizon problem with 600 years and assuming the last 300 years have fixed policy with $\mu_{t,i} \equiv 0$, $P_{t,i} \equiv P_{t,300}$, and both $c_{t,i} L_{t,i}/Y_{t,i}$ and $I_{t,i}/Y_{t,i}$ are constant for $t \geq 301$. We then solve this finite-horizon optimal control problem with CONOPT in GAMS.

Figure 10 shows the optimal climate policy paths in this century. From the top-left panel of Figure 10, we see that the social cost of carbon (SCC) is equal to carbon tax for each region, while the SCC in the north region is about double of the SCC in the tropic/south region. The initial SCC is $67 per ton of carbon (/tC) for the north region and $28/tC for the tropic/south region. This happens because the north region is much richer than the tropic/south region and also has much more production, so the damage from global warming is also larger (see the top-right panel of Figure 10). The corresponding emission control rate paths are given in the bottom-left panel showing that the north region has higher emission control rates. However, the bottom-right panel of Figure 10 shows a reverse direction for the adaption rate, implying that there are much more benefits from adaptation in the already hot tropic/south region, as its marginal damage in fractions of output from one degree warming is much higher from Figure 8.

Figure 11 shows the optimal paths in the climate system and SLR. We can see the polar amplification pattern from the top-left panel of Figure 11: the atmospheric temperature in the north region reaches 3.4 ℃ in the

Figure 10: Optimal Climate Policy for the Deterministic Model
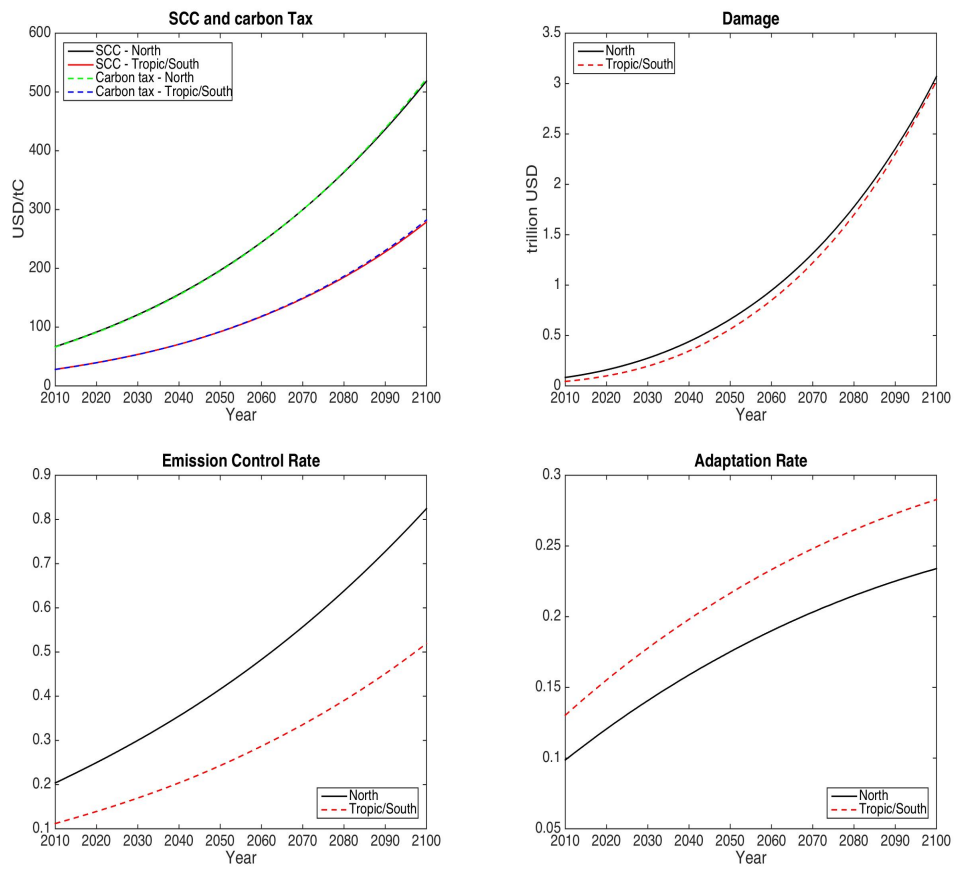
end of this century, 1.4 ℃ higher than in the tropic/south region. The top-right panel of Figure 11 shows that SLR is increasing faster and faster along the time and is a bit more than 0.6 meters in 2100. This happens because the surface temperature is higher and higher in this century so ice sheets (e.g., Greenland ice sheet, and Antarctic ice sheet) melt at higher and higher rates. The increasing temperature comes from the increasing carbon concentration in the atmosphere shown in the bottom-left panel of Figure 11. From the bottom-right panel of Figure 11, the industrial emission in the north region starts to decline soon but the tropic/south region keeps growth of emissions until 2070 as the countries in the region are poorer and want to use cheaper fossil fuel to have higher-speed economic growth. Although the global industrial emission starts to decline after 2045, the time lag between emissions and carbon concentration in the atmosphere, M_t^{AT}, makes M_t^{AT} to keep increasing in this century (there is also a time lag between between M_t^{AT} and temperatures: after 2110, M_t^{AT} starts to decrease but two regional atmospheric temperatures and ocean temperature keep increasing).

Figure 12 shows the optimal solutions in the economic system. From the left panel of Figure 12, we see that the per-capita consumption growth in the tropic/south region starts at 2.9% in the initial year and ends at 1.6% in the end of this century, while the north region has much lower growth, starting at 2.1% and ends at 1.15% in 2100. The difference of two growth paths is caused by the spillover effect of technology from the north to the tropic/south region. The economic interaction cost between two regions is shown in the right panel of Figure 12: both regions have less than 1% output for the economic interaction cost, while the north region is nearly stablized 0.3%, but the tropic/south region starts at 0.7% and decreases to 0.1% in 2100.

3.1 Bias from Ignoring Heat Transport and Polar Amplification

In the above model, we use the default values $\gamma_1 = 0.00654$ and $\gamma_2 = 0.05314$. Here "default values" refers to values of parameters set by our calibrations

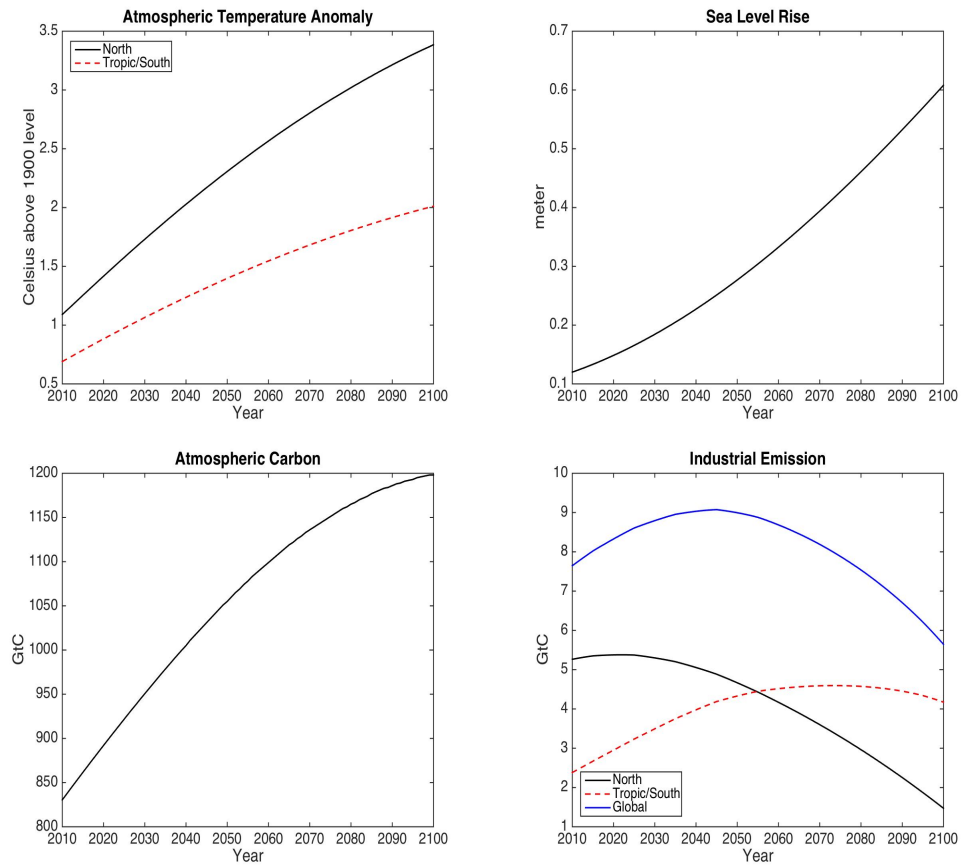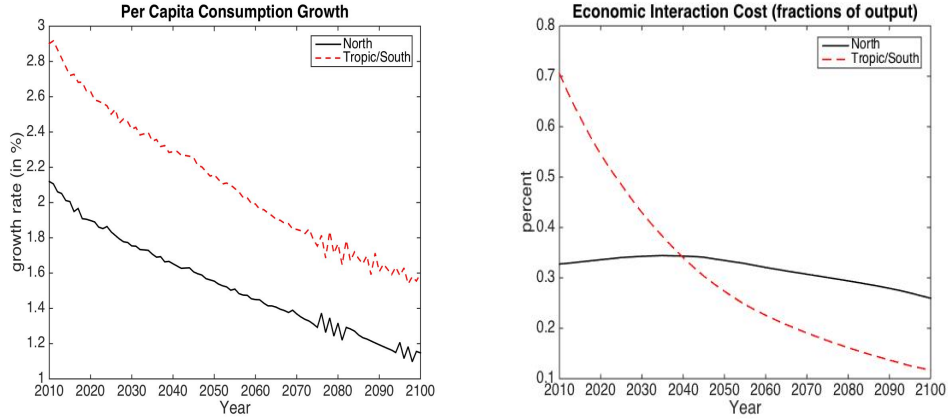Figure 11: Solutions in the Climate System of the Deterministic Model

Figure 12: Solutions in the Economic System of the Deterministic Model

to represent the spatial heat and moisture transport. Langen and Alexeev (2007) choose parameter settings of γ_1 and γ_2 at the level of abstraction associated with use of the two-box model in their sea surface temperature experiments (see also Alexeev et al 2005). In our model, we chose $\gamma_1 = 0.00654$ and $\gamma_2 = 0.05314$ as well as other related parameter values in the temperature subsystem to match the data of four RCP scenarios (after aggregation over two regions), RICE path (after aggregation over the RICE subregions for each of our regions), historical spatial data, and predictive spatial data in IPCC (2013). See Section 2.1.2 for more details for calibration in the temperature module.

Figure 13 compares the optimal solutions using $\gamma_1 = \gamma_2 = 0$ (i.e., ignoring spatial heat and moisture transport and polar amplification) with the above solutions using default γ_1 and γ_2. In each panel of Figure 13, black and red lines represent solutions in the north and tropic/south regions respectively, while the solid lines are for the default case (i.e., $\gamma_1 = 0.00654$ and $\gamma_2 = 0.05314$) and the broken lines are for $\gamma_1 = \gamma_2 = 0$. The top-left panel of Figure 13 shows that the optimal SCC paths from ignoring heat transport are higher than those with heat transport. For example, in the initial year, the SCC is \$77/tC in the north region, 15% higher than its corresponding value with heat transport, and is \$33/tC in the tropic/south region, 18%

higher than its corresponding value with heat transport. By ignoring the heat and moisture transport, we see that the north and tropic/south atmospheric temperature anomaly paths merge after 2030 in the top-right panel of Figure 13, which are between the paths of two regions with heat transport. That is, without the transport phenomena, we cannot see the polar amplification, and the temperature anomaly in the north region is underestimated while the temperature anomaly in the tropic/south region is overestimated. This implies that the solutions without heat transport will underestimate the damage in the north, and overestimate the damage in the tropic/south, which is shown in the bottom-left panel of Figure 13. The bias also exists in the optimal adaptation rates shown in the bottom-right panel of Figure 13: without heat transport, the adaptation rates in the north region will be underestimated as its corresponding atmospheric temperature anomaly is underestimated, and the adaptation rates in the tropic/south region will be overestimated as its corresponding atmospheric temperature anomaly is overestimated.

4   Stochastic Model

There are a large number of uncertainties in the model. DSICE (Cai et al. 2015a) discusses two types of risks: climate and economic risks, and also deals with parameter uncertainty over IES and risk aversion using uncertainty quantification. Cai et al (2015b) apply DSICE to include ecosystem risks, and Lontzek et al. (2015) and Cai et al. (2016) use DSICE to study the impact of tipping points on the carbon tax policy.

4.1   Tipping Point

In this paper, we assume that there is a representative tipping element that will take D years to fully unfold its damage after it happens. The final damage level is $\overline{J}$ in fraction of output, and the tipping probability depends on the contemporaneous atmospheric temperature in the north region. Let J_t represent the damage level of the tipping element, and let χ_t be the

Figure 13: Bias of Optimal Solutions from Ignoring Heat Transport and Polar Amplification
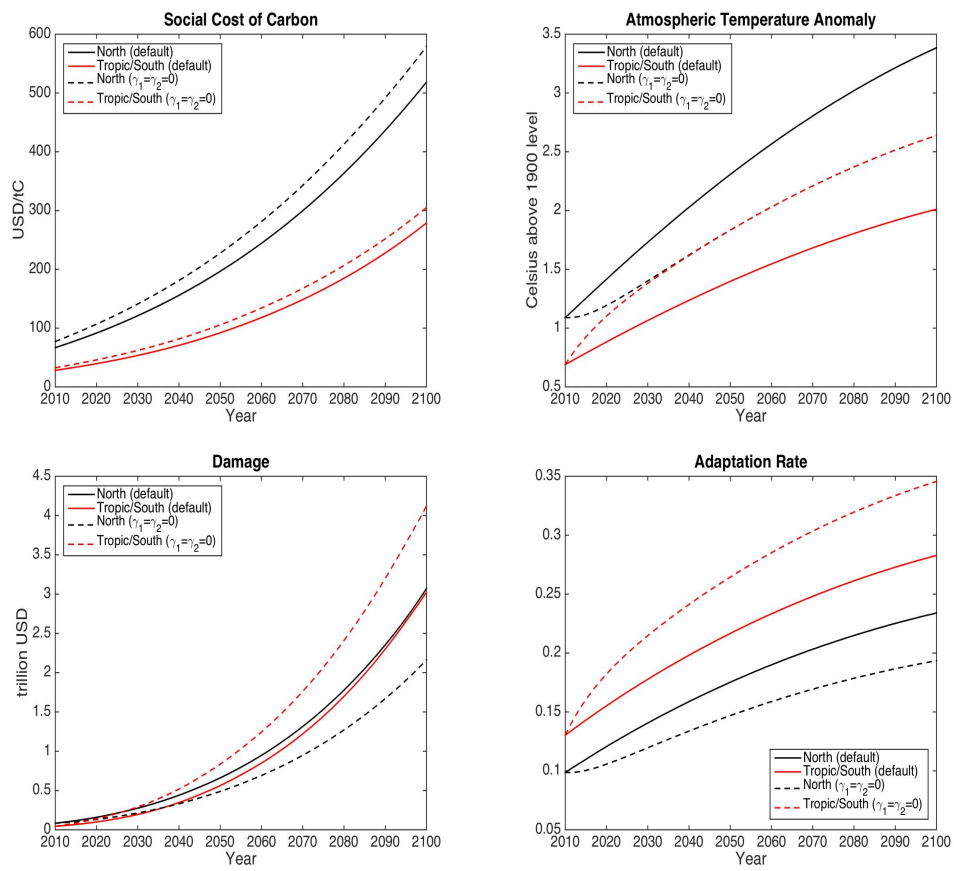
indicator representing whether the tipping event has happened or not, so $\chi_t = 0$ means that the tipping event has not happened, and $\chi_t = 1$ means that it has happened. Thus, the transition law of J_t is

$$J_{t+1} = \min(\overline{J}, J_t + \Delta)\chi_t \tag{14}$$

where $\Delta = \overline{J}/D$ is the annual increment of damage level after the tipping happens, and χ_t is a Markov chain with the following probability transition matrix

$$\begin{bmatrix} 1 - p_t & p_t \\ 0 & 1 \end{bmatrix}$$

where p_t is the tipping probability from state $\chi_t = 0$ to $\chi_t = 1$. We let

$$p_t = \exp\left(\lambda \max\left(0, T_{t,1}^{\mathrm{AT}} - 1\right)\right)$$

where λ is the hazard rate.

We use the Atlantic Meridional Overturning Circulation (AMOC) as the representative tipping element, and employ its default setup in Cai et al. (2016), that is, $D = 50$, $\overline{J} = 0.15$, and $\lambda = 0.00063$. For its generality, we let

$$\chi_{t+1} = g(\chi_t, \mathbf{T}_t, \omega_t) \tag{15}$$

denote the transition law for χ_t. The output net of all damage including SLR, temperature anomaly, and tipping becomes

$$Y_{t,i} \equiv \frac{(1 - J_t)\mathcal{Y}_{t,i}}{1 + D_{t,i}^{\mathrm{S}} + (1 - P_{t,i})D_{t,i}^{\mathrm{T}}}, \tag{16}$$

4.2 Epstein–Zin preference

We use Epstein–Zin preference (Epstein and Zin 1989) to isolate the IES and risk aversion for the stochastic model. With the similar transformation as in Cai et al. (2015a), we solve the following Bellman equation:

$$V_t(\mathbf{x}_t) = \max_{I_{t,i}, c_{t,i}, \mu_{t,i}, P_{t,i}} \quad \sum_{i=1}^{2} \tau_{t,i} u(c_{t,i}) L_{t,i} + \beta \left[\mathbb{E}_t \left\{ V(\mathbf{x}_{t+1})^{\Lambda} \right\} \right]^{1/\Lambda} \quad (17)$$

subject to (1), (4), (5), (9), (11), (14), (15), and (16), where

$$\mathbf{x}_t = (K_{t,1}, K_{t,2}, M_t^{\mathrm{AT}}, M_t^{\mathrm{UO}}, T_{t,1}^{\mathrm{AT}}, T_{t,2}^{\mathrm{AT}}, T_t^{\mathrm{OC}}, S_t, J_t, \chi_t)$$

is the vector of state variables, $\mathbb{E}_t$ is the expectation operator conditional on the time-t information, and

$$\Lambda \equiv \frac{1 - \gamma}{1 - 1/\psi}$$

where ψ is the IES (here we assume $\psi > 1$), and γ is the risk aversion parameter. We use $\psi = 1.5$ and $\gamma = 3.066$ as in Pindyck and Wang (2013) for our benchmark stochastic case.

5 Results for Stochastic Model

We solve the Bellman equation (17) using parallel dynamic programming (Cai et al. 2015c) via backward induction on the Blue Waters supercomputer. After we solve the Bellman equation, we use the optimal policy functions to generate 10,000 simulation paths forward. That is, each simulation path starts at the observed initial states, we simulate one sample of the shock for the tipping point at time t, and then with the realized sample and the optimal control policy at t, we obtain the optimal states at $t + 1$.

The two top panels of Figure 14 show the distributions of the simulated optimal social cost of carbon (SCC) for both regions. Each panel (in all figures below) includes two lines representing two deterministic cases with IES equal to 0.667 or 1.5. The shaded area represents the range of the 10,000 sample paths, and we give the average, 1%, 2% and 5% quantile paths (that is, at each time, we compute the average and these quantiles of 10,000 values). We see that the initial SCC increases significantly from the

deterministic case with $\psi = 0.667$ to the deterministic case with $\psi = 1.5$, and then increases significantly again from the deterministic case with $\psi = 1.5$ to the stochastic case with $\psi = 1.5$ and $\gamma = 3.066$. The initial SCC for the stochastic case is up to around \$270 for both regions, about 4 times as high as in the deterministic case with $\psi = 0.667$ for the north region, nearly 10 times for the tropic/south region. The cumulative probability that the tipping event happens before 2100 is only 5%, the 1% probability of tipping is year 2044, and the 2% probability is year 2061. Once the tipping event happens, the social cost of carbon immediately jump down significantly although the damage just starts to unfold in 50 years shown in the bottom-left panel of Figure 14 for the tipping damage level J_t. This happens because the high SCC before tipping has one intention to prevent or delay the tipping point as its occurrence depends on the contemporaneous temperature, but after the tipping event happens, this incentive goes away as the damage will unfold in a deterministic way. We also plot the picture of SLR in the bottom-right panel of Figure 14, showing that in the end of this century, we have 95% probability that SLR will be about 0.1 meter lower than the deterministic case with $\psi = 0.667$.

Figure 15 shows the distributions of the optimal simulation paths for atmospheric temperatures and adaptation rates in both regions for the stochastic model. We see again that the north region has much higher temperature anomaly than the tropic/south region by comparing two top panels of Figure 15 for the stochastic solutions. Moreover, it has 95% probability that the atmospheric temperature anomaly in the stochastic case is more than one ℃ lower than the deterministic case with $\psi = 0.667$ in the north region, and about 0.7 ℃ lower in the tropic/south region. Two bottom panels of Figure 15 show the optimal adaptation rates. We see again that the north region has lower adaptation rates than the tropic/south region for the stochastic solutions, and the stochastic results have lower rates than the deterministic cases, as with the higher SCC and then the lower temperatures in the stochastic case, we have lower needs to adapt.

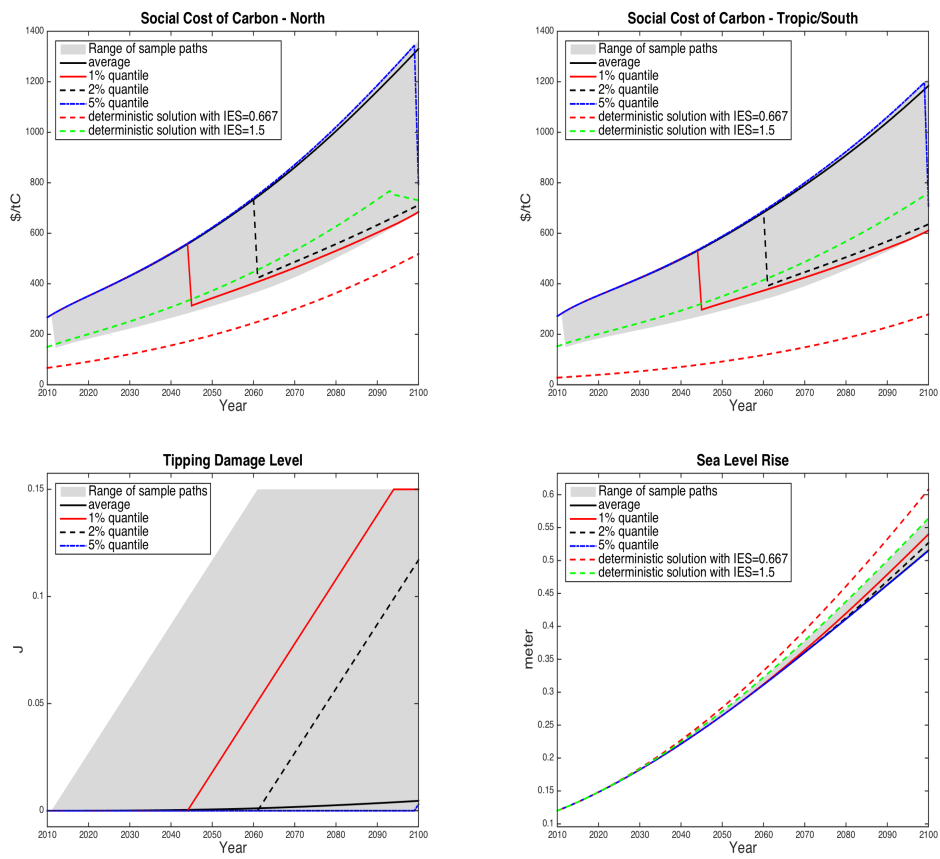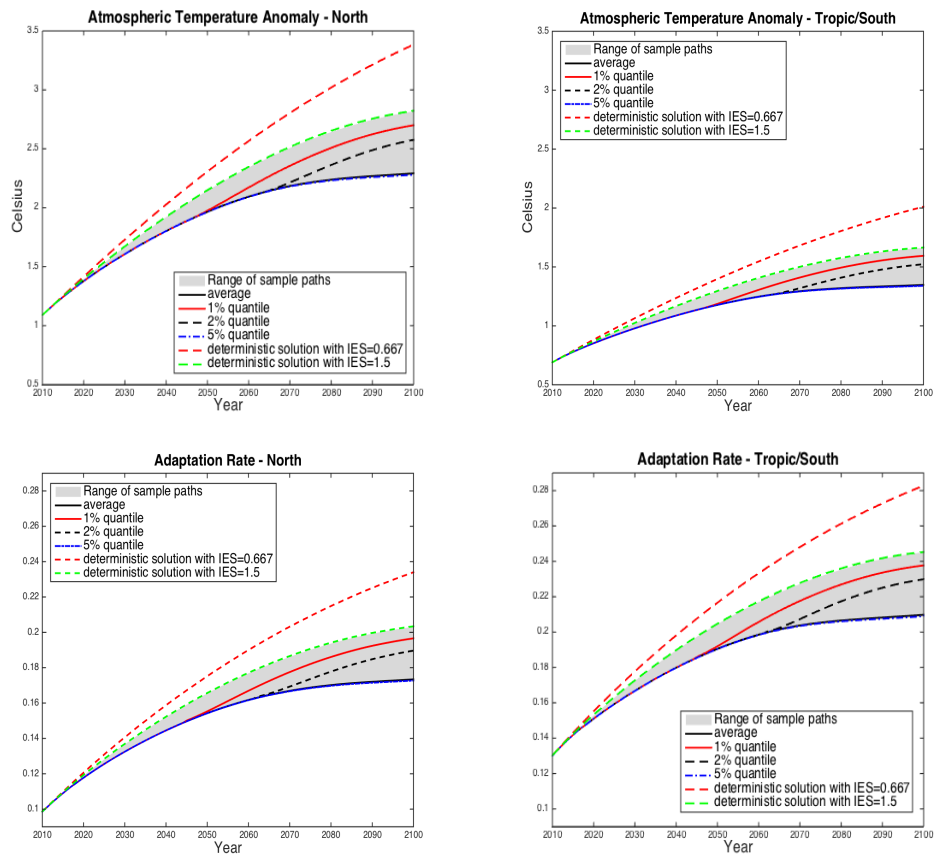Figure 14: Optimal SCC, Tipping Damage Level, and SLR for the Stochastic Model

Figure 15: Atmospheric Temperature and Adaptation Rate for the Stochastic Model

## 5.1 Bias from Ignoring Heat Transport and Polar Amplification

We examine the bias from ignoring heat and moisture transport and polar amplification (i.e., $\gamma_1 = \gamma_2 = 0$) again for the stochastic case, shown in Figure 16. In each panel of this figures, we use the black lines to represent the average paths, and the red lines for the 1% quantile paths, while the broken lines are for the case ignoring heat and moisture transport and polar amplification, and the solid lines are for the case with the default values (i.e., $\gamma_1 = 0.00654$ and $\gamma_2 = 0.05314$).

The two top panels of Figure 16 show that ignoring heat transport and polar amplification underestimates the SCC's for both north and tropic/south regions. For example, the initial SCC with $\gamma_1 = \gamma_2 = 0$ is about 10% less than in the default case for both regions. Note that this is in the opposite direction to the deterministic case shown in the top-left panel of Figure 13 where ignoring heat transport increases the SCC. This opposite direction happens because ignoring heat transport will lead to a lower temperature in the north region (shown in the bottom-left panel of Figure 16) and then underestimate the tipping probability which depends on the atmospheric temperature in the north region. This is also reflected in the 1% quantile paths: the case ignoring heat transport has a 1% cumulative probability of tipping is at year 2059, 15 years later than in the default case. With this lower tipping probability, it means less risky and then leads to smaller SCC.

6   Conclusion

Our paper has taken a first step towards including the neglected force of dynamic heat and moisture transport from the lower latitudes to the higher latitudes towards the Poles into computational Integrated Assessment Models (IAMs) used in policy relevant climate economics. We divided the world into "North" and "Tropic/South" where "North" is the region from 30°N latitude to the north pole, and "Tropic/South" is the rest. Our temperature anomaly dynamics for North and Tropic/South has two key parameters mo-

Figure 16: Bias of Solutions from Ignoring Heat Transport and Polar Amplification for the Stochastic Model
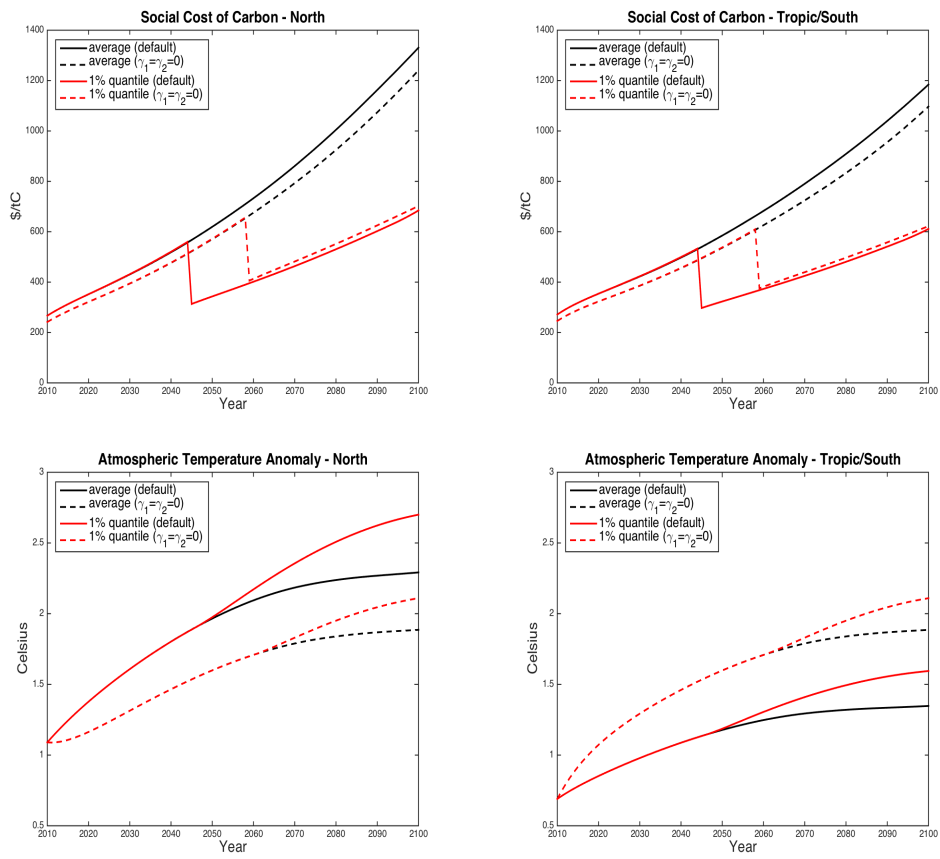
tived by Langen and Alexeev's (2007) two box model which we calibrated to $\gamma_1 = 0.00654$ and $\gamma_2 = 0.05314$. The impact of neglecting heat and moisture transport on the optimal paths of key quantities, e.g. the SCC, emission, adaptation, and damage can be assessed in our model by setting $\gamma_1 = \gamma_2 = 0$ and observing how the optimal paths change.

As one can see from Sections 3.1 and 5.1 (and Figures 13 and 16) the biases from neglecting heat and moisture transport are quite substantial. Note that we have abstracted from the nonlinearity caused by Surface Albedo Feedback (SAF) in this paper. SAF is likely to add even larger effects than what we see in Figure 13 because its effects are in the same direction. Substantial biases from neglecting heat and moisture transport are likely to remain when further research produces more realistic damage functions rather than the crude damage functions used here. See Burgess et al. (2014), Burke and Emerick (2015) for interesting recent work on constructing and estimating more realistic damage functions.

The direction of the biases in the anomalies in North and Tropic/South are expected. We are less confident about the direction of biases for the other variables except that we expect future research to also show substantial biases in the other variables when heat and moisture transport are neglected in welfare optimization. Barraca et al. (2015) showed remarkable reduction of damages to morbidity and mortality due to heat stress in the U.S. Burgess et al. (2014) showed large negative effects of extreme heat days in India, especially in rural areas. Lack of access to air conditioning is a part of the difference between India and the U.S. These results suggest that since many areas in the Tropic/South in our model are poorer than the North we might expect adaptation to be slower in the Tropic/South than in the North. Since ignoring polar transport results in some of the increased heat due to global warming not being moved towards the poles it makes sense that it is socially optimal for the Tropic/South to adapt faster when heat and moisture transport is neglected. We see this intuition supported in Figure 13.

We view this paper as taking an important step forward in calibrated IAM's at the "coarse grained" level of aggregation as RICE (Nordhaus 2010), DICE 2013R (Nordhaus and Sztorc 2013) and DSICE (Cai et al. 2015a) to

34

include the directional heat and moisture transport from regions closer to the Equator towards regions closer to the Poles. When our model is calibrated to data we found substantial biases in key quantities, temperature anomalies, emission rates, adaptation rates, and damages when a social planner neglects poleward heat and moisture transport. We also showed how potential arrival times of tipping elements in the high latitudes were affected.

References

[1] Alexeev, V.A., Langen P. L., and Bates J.R. (2005). Polar amplification of surface warming on an aquaplanet in "ghost forcing" experiments without sea ice feedbacks. Climate Dynamics, 24: 655–666.

[2] Anderson, J.E., and E. van Wincoop (2001). Borders, Trade and Welfare. NBER working paper 8515.

[3] Arrhenius, S. (1896). On the influence of carbonic acid in the air upon the temperature of the ground. Philosophical Magazine and Journal of Science, series 5, volume 41, 237–276.

[4] Alan Barreca, Karen Clay, Olivier Deschenes, Michael Greenstone and Joseph S. Shapiro (2015). Adapting to Climate Change: The Remarkable Decline in the U.S. Temperature-Mortality Relationship over the 20th Century. Available on Greenstone's website at University of Chicago.

[5] Bekryaev, R., Polyakov, I., Alexeev, V. (2010). Role of polar amplification in long-term surface air temperature variations and modern arctic warming. Journal of Climate 23, 3888–3906.

[6] Brock, W., and A. Xepapadeas (2016). Spatial Heat Transport, Polar Amplification and Climate Change Policy. Working paper.

[7] Marshall Burke and Kyle Emerick (2015). Adaptation to Climate Change: Evidence from US Agriculture. Working paper.

[8] Robin Burgess, Olivier Deschenes, Dave Donaldson, Michael Greenstone (2014). The Unequal Effects of Weather and Climate Change: Evidence from Mortality in India, London School of Economics, `http://www.lse.ac.uk/economics/people/facultyPersonalPages/facultyFiles/RobinBurgess/UnequalEffectsOfWeatherAndClimateChange140514.pdf`

[9] Cai, Y., K.L. Judd, and T.S. Lontzek (2015a). The social cost of carbon with economic and climate risks. Working paper, arXiv preprint arXiv:1504.06909.

[10] Cai, Y., K.L. Judd, T.M. Lenton, T.S. Lontzek, and D. Narita (2015b). Environmental tipping points significantly affect the cost-benefit assessment of climate policies. PNAS 112(15): 4606–4611.

[11] Cai, Y., K.L. Judd, G. Thain, and S. Wright (2015c). Solving dynamic programming problems on computational grid. Computational Economics, 45(2): 261–284.

[12] Cai, Y., T.M. Lenton, and T.S. Lontzek (2016). Risk of multiple interacting tipping points should encourage rapid CO2 emission reduction. Nature Climate Change 6, 520–525.

[13] de Bruin, K.C., R.B. Dellink, R.S.J. Tol (2009). AD-DICE: an implementation of adaptation in the DICE model. Climatic Change 95:63–81.

[14] Den Haan, W.J., K.L. Judd and M. Juillard (2011). Computational suite of models with heterogeneous agents II: Multi-country real business cycle models. *Journal of Economic Dynamics and Control*, 35, 175–177.

[15] Dennig, F., M.B. Budolfson, M. Fleurbaey, A. Siebert, and R.H. Socolow (2015). Inequality, climate impacts on the future poor, and carbon prices. PNAS, DOI 10.1073/pnas.1513967112.

[16] Desmet, K., and E. Rossi-Hansberg (2014). Spatial development. American Economic Review 104(4): 1211–1243.

[17] Desmet, K., and E. Rossi-Hansberg (2015). On the spatial economic impact of global warming. Journal of Urban Economics 88, 16–37.

[18] Eaton, J., and S. Kortum (2002). Technology, geography, and trade. Econometrica, 70(5): 1741–1779.

[19] Epstein, L.G., and S.E. Zin (1989). Substitution, risk aversion, and the temporal behavior of consumption and asset returns: a theoretical framework. *Econometrica*, 57(4), 937–969.

[20] Francis, J., Skific, N. (2015). Evidence linking rapid Arctic warming to mid-latitude weather patterns. Philosophical Transactions of the Royal Society A, 373.

[21] Francis, J., Vavrus, S. (2014). Evidence for a wavier jet stream in response to rapid Arctic warming. Environmental Research Letters 10, 1–12.

[22] Gabaix, X. (2012). Variable rare disasters: An exactly solved framework for ten puzzles in macro-finance, The Quarterly Journal of Economics, (2012) 127, 645–700.

[23] Kenneth Gillingham, William Nordhaus, David Anthoff, Geoffrey Blanford, Valentina Bosetti, Peter Christensen, Haewon McJeon, John Reilly and Paul Sztorc (2015). Modeling Uncertainty in Climate Change: A Multi-Model Comparison. Working paper.

[24] Goulder, L.H., M.A.C. Hafstead, and R.C. Williams III (2014). General Equilibrium Impacts of a Federal Clean Energy Standard. Working paper.

[25] Michael Greenstone, Elizabeth Kopits, and Ann Wolverton (2013). Developing a Social Cost of Carbon for US Regulatory Analysis: A Methodology and Interpretation, Review of Environmental Economics and Policy, 7(1): 23–46, doi:10.1093/reep/res015

[26] IPCC (2013). Climate Change 2013, The Physical Science Basis. Cambridge University Press, New York.

[27] Kang, S.M., R. Seager, D.M.W. Frierson, and X. Liu (2015). Croll revisited: Why is the northern hemisphere warmer than the southern hemisphere? Climate Dynamics, 44(5): 1457–1472.

[28] Lontzek, T.S., Y. Cai, K.L. Judd, and T.M. Lenton (2015). Stochastic integrated assessment of climate tipping points indicates the need for strict climate policy. Nature Climate Change 5, 441-444.

[29] Langen, P.L., and V. A. Alexeev (2007). Polar amplification as a preferred response in an idealized aquaplanet GCM. Climate Dynamics 29(2): 305–317.

[30] V. N. Livina and T. M. Lenton (2013). A recent tipping point in the Arctic sea-ice cover: abrupt and persistent increase in the seasonal cycle since 2007, The Cryosphere, 7, 275–286.

[31] Timothy M. Lenton and Hywel T.P. Williams (2013). On the origin of planetary-scale tipping points, Trends in Ecology & Evolution, July, Vol. 28, No. 7.

[32] Timothy M. Lenton and Joachim Schellnhumber (2007). Tipping the scales, Nature Reports, Climate Change, December, Vol. 1, 97-98.

[33] Nerem, R. S., D. P. Chambers, C. Choe, and G. T. Mitchum (2010). Estimating mean sea level change from the TOPEX and Jason altimeter missions. Mar. Geodesy, 33, 435–446.

[34] Nordhaus, W. (2010). Economic aspects of global warming in a post-Copenhagen environment. PNAS 107(26): 11721–11726.

[35] Nordhaus, W. (2013). The Climate Casino: Risk, Uncertainty, and Economics for a Warming World. Yale University Press.

[36] Nordhaus, W. (2014). Estimates of the Social Cost of Carbon: Concepts and Results from the DICE-2013R Model and Alternative Approaches, Journal of the Association of Environmental and Resource Economists, Vol. 1, No. 1/2 (Spring/Summer 2014), pp. 273-312.

[37] Nordhaus, W. (2015). Climate Clubs: Overcoming Free-riding in International Climate Policy, American Economic Review 2015, 105(4): 1339–1370 http://dx.doi.org/10.1257/aer.15000001

[38] Nordhaus, W., and P. Sztorc (2013). DICE 2013R: Introduction and User's Manual. Technical Report, Yale University.

[39] Obstfeld, M. (2004). Globalization, Macroeconomic Performance, and the Exchange Rates of Emerging Economies. NBER working paper 10849.

[40] Pierrehumbert, R.T. (2014). Short-Lived Climate Pollution. Annual Review of Earth and Planetary Sciences 42: 341–379.

[41] Pindyck, R.S., and N. Wang (2013). The economic and policy consequences of catastrophes. American Economic Journal: Economic Policy, 5(4): 306–339.

[42] Rezai, A., van der Ploeg F. (2015). Cumulative Emissions, Unburnable Fossil Fuel and the Optimal Carbon Tax. CEEES paper CE3S-07/15.

[43] Sachs, J.D. (2001). Tropical underdevelopment. NBER working paper 8119.

[44] Schaefer, K., Lantuit, H., Romanovsky, V.E., Schuur, E.A.G., Witt, R. (2014). The impact of the permafrost carbon feedback on global climate. Environmental Research Letters 9, doi:10.1088/1748-9326/9/8/085003.

[45] Serreze, M., Barry, R. (2011). Processes and impacts of Arctic amplification: a research synthesis. Global and Planetary Change 77, 85–96.

[46] Schuur, E.A.G., McGuire, A.D., Schadel, C., Grosse, G., Harden, J.W., Hayes, D.J., Hugelius, G., Koven, C.D., Kuhry, P., Lawrence, D.M., Natali, S.M., Olefeldt, D., Romanovsky, V.E., Schaefer, K., Turetsky, M.R., Treat, C.C., Vonk, J.E. (2015). Climate change and the permafrost carbon feedback. Nature 520, 171–179.

[47] Stephens, G.L., D. O'Brien, P. J. Webster, P. Pilewski, S. Kato, and J.-l. Li (2015). The albedo of Earth. Review of Geophysics, 53(1): 141–163.